AGU ADVANCING EARTH AND SPACE SCIENCES

Earth and Space Science

RESEARCH ARTICLE
10.1029/2024EA003630

The Benefits of Future Quantum Accelerometers for Satellite Gravimetry

P. Zingerle[1], M. Romeshkani[2], J. Haas[3], T. Gruber[1], A. Güntner[3,4], J. Müller[2], and R. Pail[1]

[1]Institute of Astronomical and Physical Geodesy, Technical University of Munich, Munich, Germany, [2]Institut für Erdmessung, Leibniz Universität Hannover, Hannover, Germany, [3]Helmholtz Centre Potsdam GFZ German Research Centre for Geosciences, Section Hydrology, Potsdam, Germany, [4]Institute of Environmental Science and Geography, University of Potsdam, Potsdam, Germany

Key Points:

- Quantum instruments may significantly improve the sensitivity of gravity measurements
- A higher sensitivity cannot substantially improve current and upcoming satellite gravity missions due to temporal aliasing

Correspondence to:
P. Zingerle,
zingerle@tum.de

Citation:
Zingerle, P., Romeshkani, M., Haas, J., Gruber, T., Güntner, A., Müller, J., & Pail, R. (2024). The benefits of future quantum accelerometers for satellite gravimetry. *Earth and Space Science*, *11*, e2024EA003630. https://doi.org/10.1029/2024EA003630

Received 14 MAR 2024
Accepted 3 AUG 2024

Author Contributions:
Conceptualization: P. Zingerle, M. Romeshkani, J. Haas, T. Gruber, A. Güntner, J. Müller, R. Pail
Data curation: P. Zingerle, M. Romeshkani, J. Haas
Formal analysis: P. Zingerle, M. Romeshkani, J. Haas
Funding acquisition: T. Gruber, A. Güntner, J. Müller, R. Pail
Investigation: P. Zingerle, M. Romeshkani, J. Haas, A. Güntner
Methodology: P. Zingerle, M. Romeshkani, J. Haas
Project administration: P. Zingerle
Software: P. Zingerle, M. Romeshkani, J. Haas
Supervision: T. Gruber, A. Güntner, J. Müller, R. Pail
Validation: P. Zingerle, M. Romeshkani, J. Haas
Visualization: P. Zingerle, M. Romeshkani, J. Haas
Writing – original draft: P. Zingerle, M. Romeshkani, J. Haas
Writing – review & editing: P. Zingerle, M. Romeshkani, J. Haas, T. Gruber, A. Güntner, J. Müller, R. Pail

Abstract We investigate the benefits of future quantum accelerometers based on cold atom interferometry (CAI) on current and upcoming satellite gravity mission concepts. These mission concepts include satellite-to-satellite tracking (SST) in a single-pair (GRACE-like) and double-pair constellation as well as satellite gravity gradiometry (SGG, single satellite, GOCE-like). Regarding instruments, four scenarios are considered: current-generation electrostatic (GRACE-, GOCE-like), next-generation electrostatic, conservative hybrid/CAI and optimistic hybrid/CAI. For SST, it is shown that temporal aliasing poses currently the dominating error source in simulated global gravity field solutions independent of the investigated instrument and constellation. To still quantify the advantages of CAI instruments on the gravity functional itself, additional simulations are performed where the impact of temporal aliasing is synthetically reduced. When neglecting temporal aliasing, future accelerometers in conjunction with future ranging instruments can substantially improve the retrieval performance of the Earth's gravity field (depending on instrument and constellation). These simulation results are further investigated regarding possible benefit for hydrological use cases where these improvements can also be observed (when omitting temporal aliasing). For SGG, it is demonstrated that, with realistic instrument assumptions, one is still mostly insensitive to time-variable gravity and not competitive with the SST principle. However, due to the improved instrument sensitivity of quantum gradiometers compared to the GOCE mission, static gravity field solutions can be improved significantly.

1. Introduction

Accelerometers play a crucial role when observing gravity from space since they allow to separate gravitational from non-gravitational forces (e.g., atmospheric drag, solar pressure, etc.). Observing the Earth's gravity field from space imposes particularly high requirements on the accelerometers due to the attenuation of the gravitational signal at satellite altitude and due to the Earth's comparatively dense atmosphere, which basically introduces two complications. On the one hand, the minimum altitude of satellites is practically limited to about 250 km due to technical reasons. At such altitudes, the gravitational signal energy of smaller features is already significantly damped. On the other hand, atmospheric drag is still very prominent there. Eventually, this implies that accelerometers suitable for satellite gravity missions need to measure strong non-conservative forces (i.e., they need a wide measurement range) with very high accuracy.

In current satellite missions that observe the Earth's gravity field (gravimetry missions), electrostatic accelerometers are commonly utilized due to their minimal noise at high frequencies. However, they come with drawbacks, such as drift at low frequencies and challenges in estimating biases and scale factors. Considering these deficiencies, novel quantum sensors, specifically accelerometers based on cold atom-interferometry (CAI), may further benefit satellite gravimetry: besides their high precision and sensitivity, quantum sensors exhibit a complementary spectral behavior for improved gravity field observation (Knabe et al., 2022; Lévèque et al., 2022; Meister et al., 2022).

Up until now, several dedicated satellite gravity missions have been successfully conducted. Noteworthy among these are their latest and most performant realizations, namely the GOCE mission (Drinkwater et al., 2003) and the GRACE/-FO mission (Flechtner et al., 2017; Kornfeld et al., 2019; Tapley et al., 2004). The former (GOCE) is based on the satellite gravity gradiometry (SGG) concept, where the gravitational gradient is directly observed by an ensemble of accelerometers aligned in a 3D array. The latter (GRACE/-FO) is based on the low-low satellite-

to-satellite tracking (SST) concept where two satellites are located on similar orbits in close vicinity to each other (about 220 km in the case of GRACE/-FO) and observe the variation in their inter-satellite distance with very high accuracy (e.g., through a micro-wave or laser instrument). Both concepts have their advantages and disadvantages: SGG requires only one satellite, relies solely on gradiometers/accelerometers and is conceptually more sensitive to shorter wavelengths of the gravity field. However, as of yet, gradiometers are not sensitive enough to achieve a comparable performance to SST in the longer wavelengths. For the highest accuracy in the longer wavelengths, SST is currently without competition and the only concept capable of detecting (non-tidal) time-variable changes in the Earth's gravity field from space. Due to their individual strengths, both concepts are viable options for future satellite gravity missions. Also, both concepts rely heavily on their accelerometer performance, which is why they will possibly benefit from CAI instruments. For SGG, an ensemble of accelerometers, placed outside of the satellite's center of mass, observe non-gravitational as well as gravitational accelerations (gravity gradients). In case of SST, one accelerometer is usually located at the center of mass of each satellite to measure only the non-gravitational accelerations which are needed to separate the gravitational component from the ranging observation.

Recognizing the potential of CAI instruments for satellite gravity missions, this contribution strives to quantify the possible benefit of future hybrid/CAI accelerometers on current and upcoming SGG resp. SST mission designs (see, e.g., Heller-Kaikov et al., 2023; Daras et al., 2024). To achieve this, the paper is structured as follows: firstly, an overview of the investigated instruments (classical/hybrid/CAI) is provided, and the thereof derived instrument (mission) scenarios (SST and SGG) are described (Section 2). Then, the SST mission simulator setup and the simulation results of the previously defined SST instrument scenarios are presented for a future single- and double-pair constellation (Section 3). In Section 4, the corresponding SGG mission simulator is introduced, and the appropriate (single-satellite) SGG mission simulation results are shown and interpreted. Subsequently, in Section 5, special attention is given to quantify the benefit on hydrological use cases when applying the simulated time-variable gravity field solutions, which have been previously obtained (within Section 3). Eventually, the main conclusions of this work are summarized in Section 6.

2. Instrument Scenarios

In this section, the different instrument scenarios investigated in this contribution are described. Since SST as well as SGG missions require accelerometers, the different considered accelerometers (for both concepts) are intruded in a first step in Section 2.1. To eventually enable a comparison between current and future accelerometers, several different possible accelerometer types are taken into consideration (classical electrostatic and future hybrid/CAI). Subsequently, based on these accelerometers, concrete instrument scenarios for SST missions (including ranging instruments, see Section 2.2) and for SGG missions (i.e., gradiometers, see Section 2.3) are derived.

2.1. Accelerometers

Electrostatic accelerometers. One limitation in current satellite gravimetry missions with significant error contribution at lower frequencies is caused by the drift of the EA (Christophe et al., 2015; Kupriyanov et al., 2024). Thus, two advanced electrostatic accelerometers are studied, which are characterized by enhanced accuracy and spectral sensitivity. The first one is associated with the positive results achieved through the LISA Pathfinder mission, where the sensor behavior has been adapted for low Earth orbits (Armano et al., 2018). Alvarez et al. (2022) designed a scaled-down LISA Pathfinder accelerometer for superior performance in upcoming satellite gravimetry missions with two different approaches. One assumes a drag-free system operating at 350 km altitude (*Alvarez@350*). Its (one-sided) amplitude spectral density (ASD) is given by

$$acc_{A@350}(f) = 3 \cdot 10^{-8} \cdot f^2 + 4 \cdot 10^{-13} \sqrt{1 + \frac{7 \cdot 10^{-4}}{f} + \left(\frac{3 \cdot 10^{-4}}{f}\right)^2} \; \frac{m}{s^2 \sqrt{Hz}}. \quad (1)$$

The second one, without drag-free system and designed for 500 km altitude (*Alvarez@500*), has the ASD

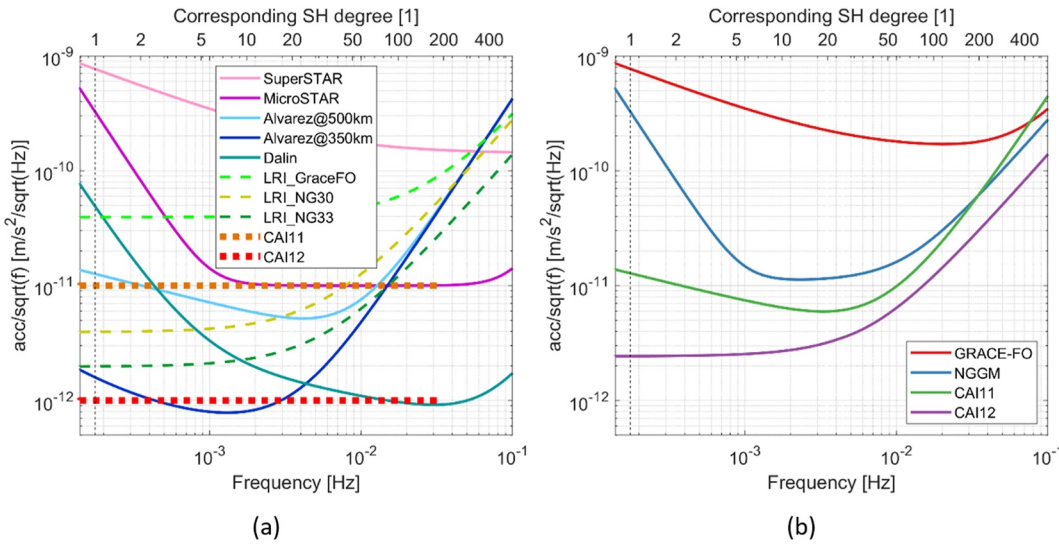

Figure 1. Amplitude spectral densities (ASDs) in terms of accelerations for different instruments: (a) ASDs of the different considered accelerometers (solid: classical electrostatic accelerometers, bold dashed: CAI) and ranging instruments (for SST scenarios, thin dashed). Accelerometer performance is normalized to line-of-sight accelerations (i.e., multiplied by $\sqrt{2}$). (b) Combined accelerometer and LRI (product) noise for the four selected SST instrument scenarios, reflecting the resulting noise behavior on the SST ranging observations.

$$acc_{A@500}(f) = 3 \cdot 10^{-8} \cdot f^2 + 5 \cdot 10^{-13} \cdot \sqrt{1 + \left(\frac{1}{f}\right)^{\frac{2}{3}}} \; \frac{m}{s^2\sqrt{Hz}}. \tag{2}$$

Another advanced EA was proposed by the French aerospace company ONERA, that was also responsible for designing and constructing the accelerometers utilized in satellite gravity missions such as GRACE, GOCE, and GRACE-FO. This accelerometer, referred to as *Dalin* (Dalin et al., 2020), is characterized by

$$acc_D(f) = 2.4 \cdot 10^{-13} \cdot \frac{1}{\sqrt[4]{f}} + 1 \cdot 10^{-18} \cdot \frac{1}{f^2} + 8 \cdot 10^{-11} \cdot f^2 \; \frac{m}{s^2\sqrt{Hz}}. \tag{3}$$

Next to these future accelerometers, also current generation instruments are considered for simulating the baseline scenarios. For the GRACE/-FO baseline scenarios, the performance of the ONERA *SuperSTAR* accelerometer (Frommknecht et al., 2003; Touboul et al., 1999) is used:

$$acc_S(f) = 1 \cdot 10^{-10}\sqrt{1 + \frac{0.005\ Hz}{f}} \quad \frac{m}{s^2\sqrt{Hz}}. \tag{4}$$

For simulating the projected performance of an upcoming next generation SST gravity field mission (NGGM, see Heller-Kaikov et al., 2023) a performance fitting the ONERA *MicroSTAR* instrument (Cesare et al., 2022; Lenoir et al., 2011) is adopted:

$$acc_M(f) = \frac{1}{\sqrt{2}} \cdot 10^{-11} \sqrt{\left(\frac{10^{-3}Hz}{f}\right)^4 \Big/ \left(\left(\frac{10^{-5}Hz}{f}\right)^4 + 1\right) + 1 + \left(\frac{f}{10^{-1}Hz}\right)^4} \; \frac{m}{s^2\sqrt{Hz}}. \tag{5}$$

It is further assumed that all accelerometers exhibit the same performance on all three axes (and/or that tilting and other introduced errors are already accounted for in the noise specification).

Figure 1a (solid curves) illustrates the ASDs of these accelerometers. Their different behaviors are evident, particularly in the low-frequency and high-frequency parts.

Table 1
Selected SST Instrument Scenarios/Classes and Not Selected Scenarios, Which Produce Very Similar Simulation Results

Acronym/Class	Selected instrument scenario	Similar scenarios
GRACE-FO—current state of the art	SuperSTAR + LRI_GraceFO	-
NGGM—next generation (currently being developed)	MicroSTAR + LRI_NG30	MicroSTAR + LRI_NG33 (for single pair) (MicroSTAR+) CAI11 + LRI_NG30 (for double pair)
CAI11—future (realistic)	Alvarez@500 km + LRI_NG33	(MicroSTAR+) CAI11 + LRI_NG33
CAI12—future (optimistic)	(Dalin+) CAI12 + LRI_NG33	Alvarez@350 km + LRI_NG33 (for single pair) Dalin + LRI_NG33 (for double pair)

Note. Instruments in brackets may be considered for technical reasons but they do not influence the product noise as assumed for simulation.

CAI accelerometers. Cold Atom Interferometry employs atoms as test masses, which are manipulated by a sequence of laser pulses to form an interferometer. The resulting phase shift of the atomic clouds following different paths is directly proportional to the acceleration acting at the system (see Abend et al., 2020 for more details). CAI accelerometers show high long-term stability and precise scale factor determination based on the frequency stability of the laser system. Earlier simulation studies using CAI sensors, as presented by Abrykosov et al. (2019) and Müller and Wu (2020), indicate a promising potential for gravity field recovery. In this study, we consider two CAI accelerometers with two different white-noise levels (cf. Figure 1a, bold dashed lines). One is denoted as the realistic CAI accelerometer that is characterized by a constant noise level of $10^{-11}\frac{m}{s^2\sqrt{Hz}}$ (CAI 11), while the other one is referred to as the future CAI accelerometer, featuring a constant noise level of $10^{-12}\frac{m}{s^2\sqrt{Hz}}$ (CAI 12).

Hybrid accelerometers. The precision and high stability of CAI-based accelerometers are promising but show some shortcomings due to dead times and a relatively constrained dynamic range (Lévèque et al., 2022). A prospective strategy to resolve these limitations in atom interferometry can be achieved by hybridization with electrostatic accelerometers (Abrykosov et al., 2019). The stable characteristics of CAI accelerometers, coupled with their lower temporal resolution, complement the high temporal resolution of EA. The synergy between CAI and electrostatic accelerometers presents a mutual advantage. CAI facilitates the calibration of electrostatic accelerometers by determining its scale factor, while electrostatic accelerometers complement CAI accelerometers by offering measurements at high frequencies beyond the operational range of CAI (Knabe, 2023). In this study, we consider therefore hybrid accelerometers where the noise characteristic is obtained by optimally combining the previously defined EA with specific appropriate CAI variants (e.g., see Table 1).

2.2. SST Instrument Scenarios

Inter-satellite ranging instruments. In case of SST, gravity field observations are obtained by measuring the distance between two satellites as they orbit the Earth next to each other using an inter-satellite ranging instrument. Since these inter-satellite measurements are still contaminated by non-gravitation forces, accelerometers in the center of mass of each satellite are additionally needed to separate the gravitation component for the final gravity field observable. Eventually, this implies that the SST principle requires not only precise accelerometers (cf. Section 2.1) but also a very accurate ranging instrument. Since the introduced accelerometer performances include projections into the future (these instruments still need to be developed), also future developments for the assumed ranging instruments have to be taken into account. Hence, three different satellite (laser) ranging instrument (LRI) performance variants are considered: Firstly, an estimate of the current generation performance of the LRI on board of GRACE-FO (LRI_GraceFO, see Hauk et al., 2023, also in terms of one-sided ASD):

$$lri_G(f) = 2.2 \cdot \frac{10^{-10}}{\sqrt{f}} + \frac{10^{-12}}{f^2}\ \frac{m}{\sqrt{Hz}}. \tag{6}$$

As second variant, a next-generation instrument, which projects the development to the year 2030 (LRI_NG30):

$$lri_{NG30}(f) = 2.2 \cdot \frac{10^{-10}}{\sqrt{f}} + \frac{10^{-13}}{f^2} \; \frac{m}{\sqrt{Hz}}. \tag{7}$$

The third variant reflects an even further projection to the year 2033 (LRI_NG33):

$$lri_{NG33}(f) = 1.1 \cdot \frac{10^{-10}}{\sqrt{f}} + \frac{5 \cdot 10^{-14}}{f^2} \; \frac{m}{\sqrt{Hz}}. \tag{8}$$

All three variants are depicted in Figure 1a (thin dashed lines) in terms of range accelerations (to be comparable with the accelerometers).

Combined instrument scenarios. Having now a set of accelerometer variants and a set of LRI variants, a new combined set has to be defined to specify the final SST instrument scenarios, which will be used for the simulations (Section 3). Even though a lot of combinations of accelerometers and LRIs are possible, only a few are reasonable: Since the ASD of the combined LRI and accelerometer noise (hereafter denoted as the *product noise*) is always dominated by the noisier component, it is reasonable to only combine instruments with comparable noise levels. Further, several different combinations may result in a very similar product noise (cf. Figure 1a). Eventually, also the degree of realism (resp. availability) between LRI and accelerometer needs to match (i.e., it is not sensible to combine the current generation accelerometers with the LRI, which just becomes available by 2033). Taking into account all these guidelines, basically four rather distinct product noise scenarios (resp. classes) can be identified where each reflects a certain degree of maturity (cf. Table 1 and Figure 1b): (a) the GRACE-FO class, reflecting the current state of the art, (b) the NGGM class, reflecting the next generation of SST missions, which is currently being developed, (c) the CAI11 class, representing a realistic future (CAI) instrumentation, and (d) the CAI12 class, which stands in place of an optimistic future (CAI) instrument development. Be aware that the acronym NGGM as used in this contribution defines an instrument class and is hence not directly related to the ESA NGGM mission (which denotes the inclined pair of the ESA/NASA double-pair MAGIC mission, see Daras et al., 2024).

When inspecting the ASDs of the combined (product) noise (Figure 1b), it is already discernible that for the higher frequencies (starting around 0.01 Hz) the LRI becomes the limiting component while for the lower frequencies the accelerometer is dominating for most combinations. Though, in case of CAI12, the LRI (even the best one) is already dominating the whole noise spectrum. This implies that for SST scenarios, improving the accelerometer even further will not result in any benefit for the final ranging observations as long as no better LRI instruments become available. Further noteworthy, the electrostatic accelerometers proposed by Alvarez et al. (2022) are very stable in the low frequency, thus, competing with the CAI instruments (which is why we put these in the same class for the CAI11 SST instrument scenario, see Table 1).

2.3. SGG Instrument Scenarios

CAI gradiometer and attitude sensors. When applying the SGG principle, an array of accelerometers (cf. Section 2.1), located symmetrically with respect to the satellite's center of mass, measure differential accelerations along their baselines which contain information about the gravity field gradient (and rotational components). Since all accelerometers are usually mounted on a rigid platform, the distances between the accelerometer pairs are assumed to be known and constant. Such an accelerometer array is commonly referred to as a gravity gradiometer. According to the operational complexity of CAI accelerometers, we assume to have only one sensitive gradiometer axis in each direction (by using six single one-axis ACCs), which is why we only use the diagonal components of the gradiometry tensor in our study. This then requires an alternative method to determine the gradiometer attitude and the angular velocities that enter he gradient observations (Siemes, 2018; Stummer et al., 2011). Here, we consider two different gyroscopes with two different noise levels. One of them has a white-noise level close to $10^{-8}\frac{rad}{s\sqrt{Hz}}$ (Douch et al., 2018) in term of angular velocity that we call realistic gyroscope (R Gyro). The second one is a CAI-based gyroscope and has different noise levels depending on its interrogation time. Here, we take it as a future gyroscope with a white-noise level close to $10^{-9}\frac{rad}{s\sqrt{Hz}}$ (Savoie et al., 2018).

Table 2
Selected Satellite Gravity Gradiometry Instrument Scenarios/Classes

Class	Selected accelerometer	Selected gyroscope
GOCE—current state of the art	3D MicroSTAR · 0.2 (i.e., about 5 times better)	Reconstructed from 3D gradiometer + R Gyro
Future EA—future 3D EA and gyroscope	3D EA[a]	
Realistic CAI—realistic 1D CAI and gyroscope	EA[a] + CAI11	R Gyro ($10^{-8}\ rad/s/\sqrt{Hz}$)
Future CAI—future 1D CAI and gyroscope	EA[a] + CAI12	CAI Gyro ($10^{-9}\ rad/s/\sqrt{Hz}$)

[a]EA (electrostatic accelerometer): {Alvarez@350, Dalin}.

Instrument classes. Considering different noise levels of (CAI) accelerometers and the utilization of different types of gyroscopes in the SGG concept, the instrument scenarios can be divided into four classes (cf. Table 2):

- The first class represents the status quo, resembling a GOCE-like instrument performance. The GOCE-like setup consists of six 3D electrostatic accelerometers where each EA has an ASD shape similar to MicroSTAR (see Figure 1a) but with an error level which is about five times lower (i.e., better, see Touboul et al., 2016). The GOCE accelerometer performance is hence only slightly worse than the future Dalin performance.
- The second class also consists of gradiometers in a GOCE-like setup (i.e., constructed through six 3D electrostatic accelerometers) but now using future EA specifications in form of (a) the Dalin and (b) the Alvarez@350 realization (cf. Figure 1a). For the first and the second class, angular velocities can be reconstructed with sufficiently high accuracy directly through the off-axis accelerations measured by the 3D electrostatic accelerometers.
- The third class comprises hybrid accelerometers, combining electrostatic accelerometers (Alvarez@350 and Dalin) with CAI11 (see Figure 1a). In this class, we use a realistic gyroscope, and given the use of both realistic hybrid accelerometers and realistic gyroscope, this class is denoted as the Realistic CAI class. Specifically, it includes (a) Alvarez@350 + CAI11 + R Gyro and (b) Dalin + CAI11 + R Gyro.
- The fourth class involves a fusion of a future hybrid accelerometer and a future gyroscope. The future accelerometer is a combination of a future EA with CAI12 (cf. Figure 1a). Given the lower noise level of CAI accelerometers, which might emerge from future technological advancements, coupled with the utilization of a CAI-based gyroscope, this category is referred to as the Future CAI class. Concretely, it includes (a) Alvarez@350 + CAI12 + CAI Gyro and (b) Dalin + CAI12 + CAI Gyro.

3. SST Simulations and Results

This section treats the implementation and evaluation of the conducted SST simulation scenarios. In Section 3.1, the simulation setup for the various scenarios will be described, while in Section 3.2 the main results will be presented and interpreted. In Section 3.3, the impact of temporal aliasing on the simulation results will be discussed in more detail by evaluating additional scenarios with reduced time-variable input signal.

3.1. SST Simulation Setup/Scenarios

SST-simulations are conducted by using an adapted version of the TUM full-scale SST simulator (Daras, 2016; Daras et al., 2015). For the SST simulations, the selected scenarios are designed to be, in most aspects, similar to current generation single-pair (GRACE/-FO) and next generation (MAGIC, being planned) double-pair SST gravity field missions.

Orbits. For the single-pair (SP) scenarios, a polar GRACE-like orbit (89° inclination, 463 km altitude) is assumed. For the double-pair (DP) scenarios, the same polar pair from the single-pair scenario is reused and combined with an additional inclined pair (70° inclination, 432 km altitude). Both constellation scenarios are designed to have (among other) a sub-cycle of 7 days in which period the ground-track pattern is nearly homogeneous. Concretely, the orbits (polar and inclined) correspond to the constellation scenario "3d_H" from the ESA NGGM/MAGIC science support study (Heller-Kaikov et al., 2023). Since the present study aims to quantify the benefit of quantum accelerometers for current and next-generation satellite gravity missions, larger satellite constellations are not considered.

Forward modeling. To enable a high degree of realism within the SST-simulations, all important (time-variable) gravity signal components are included in the forward modeling ("true world" simulation). These include a static gravity field model (*GOCO05*s, Mayer-Gürr et al., 2015), non-tidal time-variable gravity (components AOHIS from the ESA *Earth System Model, ESM*, Dobslaw et al., 2015), and a tidal gravity field model (*EOT11a*, Savcenko & Bosch, 2012). All forward modeled gravity field components are simulated up to the spherical harmonic degree and order (d/o) 120. In the following, this forward modeling scenario (including all major time-variable gravity field components) will be denoted as *full-noise* (forward) model, since the resulting gravity field models will include instrument noise as well as temporal aliasing "noise". Temporal aliasing is generated when the signal cannot be reconstructed correctly due to an insufficient sampling and/or parametrization in the time domain. Since the given full-noise forward model contains strong daily and sub-daily signal components (e.g., tides), it is expected that the temporal aliasing error plays a crucial role when estimating (static) weekly gravity fields. Next to the full-noise scenario, also the so-called *product-only* forward modeling scenario will be considered. It only contains the static (time-invariant) gravity field component (i.e., GOCO05s) and omits all time-variable parts (tidal and non-tidal). Thus, gravity field models resulting from product-only scenarios will just include the instruments (assumed as product noise, see Section 2) as error source (meaning temporal aliasing errors are excluded). This is useful when trying to assess the influence of the instruments alone on the final gravity field solution (assuming temporal aliasing could be eliminated by other means).

Backward modeling. In the SST-simulations, the gravity field is retrieved (i.e., backward-modeled) through the common least-squares adjustment approach by using a static spherical-harmonic parametrization. In the TUM full-scale SST simulator, SST ranging observations are modeled in terms of range-rates by using the integral equation approach based on short-arcs (brief *short-arc* approach, see Mayer-Gürr, 2006). In our approach the observation are stochastically modeled also on an arc-wise basis through covariance matrices computed from the instrument ASDs provided in Section 2. The default retrieval period for the gravity fields is set to 31 days, as this roughly coincides with the period used in the standard GRACE processing (for all results shown in this Section 3). For assessing the benefit for hydrological use cases (Section 5), a retrieval period of 7 days is chosen as it poses a good compromise between ground-track coverage (i.e., maximum achievable resolution) and (minimum) retrieval length for single- and double-pair SST missions. For monthly solutions and weekly double-pair solutions, the max. d/o for the retrieved gravity field model is set to 120. For weekly single-pair solutions this max. d/o is reduced to 100 (due to the limited ground track resolution). For the full-noise forward modeling scenarios, a realistic de-aliasing is performed in the backward modeling (comparable to the standard GRACE-processing) by removing non-tidal (de-aliasing products for components AO from the ESA ESM, Dobslaw et al., 2015) and tidal (*GOT4.7*, Ray, 2008) de-aliasing models prior to the gravity field retrieval.

3.2. SST Simulation Result

When applying the simulation scenarios defined in Section 3.1, one ends up with four simulations per defined instrument noise: (a) product-only/single-pair, (b) product-only/double-pair, (c) full-noise/single-pair, and (d) full-noise/double-pair. Since each of these scenario classes shows rather homogeneous behavior (in terms of retrieval performance), the simulations will be grouped according to these classes within the following discussion.

Product-only, single-pair. Figure 2 shows degree-dependent errors in terms of equivalent water heights (EWH, see, e.g., Heller-Kaikov et al., 2023) for all conducted simulations. It demonstrates that the gravity field retrieval error in case product-only scenarios scales basically directly with the instrument noise level (cf. Figure 2a, solid lines). This is to be expected, because in this case the instruments pose the only error source. Comparing the magnitudes of the single-pair product-only degree errors, large performance jumps between the different instrument scenarios are visible. Specifically, when comparing the NGGM to the CAI11 instrument scenario, a large improvement (about one order of magnitude) is discernible even though the instrument performances do not differ strongly in the high and mid-frequencies (cf. Figures 1b and 2a). However, NGGM shows much worse performance than CAI11 in the low frequencies. This indicates that, for single-pair scenarios, the instrument performance in the long wavelengths (i.e., low frequencies) is the dominant driver for the gravity field retrieval error. To further underline this finding, additional instrument scenarios have been simulated (not included in the figures for the sake of clarity) where the performance is just differing in the lower (<0.01 Hz) or higher frequencies (>0.01 Hz). These simulations have confirmed this behavior and have further shown that the impact of the instrument performance in the higher frequencies (>0.01 Hz) is minor in case of product-only single-pair scenarios.

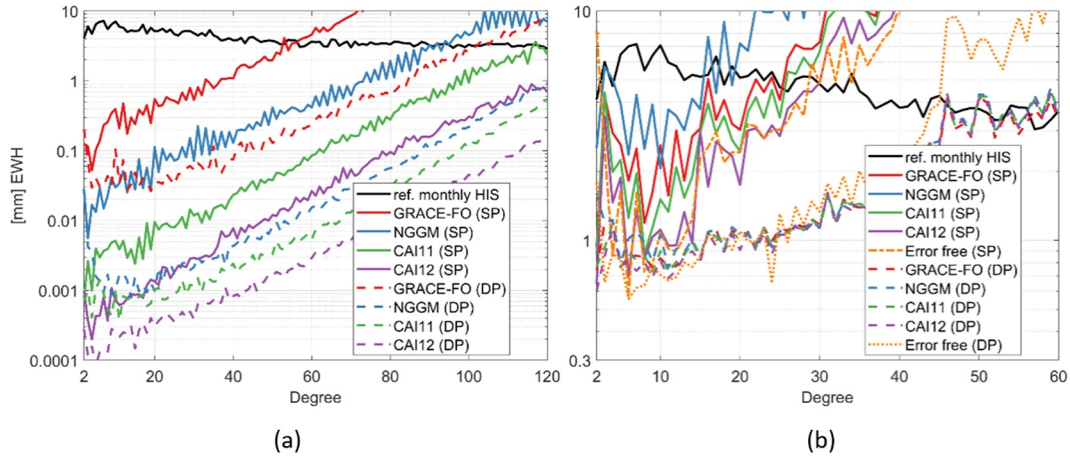

Figure 2. Degree errors in terms of equivalent water heights (EWH, see, e.g., Heller-Kaikov et al., 2023) for all conducted simulations. The black curve shows the monthly reference mean signal (ESM components HIS + AO de-aliasing errors). Colored curves correspond to the differences of the individual instrument scenarios to the reference. Solid lines depict single-pair scenarios, dashed lines double-pair scenarios. (a) Product-only scenarios for single-pair (SP) and double-pair (DP) constellations for all instrument scenarios. (b) Corresponding full-noise scenarios. Orange lines represent additional scenarios where no instrument errors are included (i.e., assuming negligible small white-noise on range-rate level).

Product-only, double-pair. Similar to the product-only single-pair scenarios, also the product-only double-pair scenarios scale with the instrument performance (cf. Figure 1a, dashed lines). All product-only double-pair instrument scenarios can outperform their single-pair counterparts by at least one order of magnitude. However, the relative decrease of the retrieval error behaves differently than in the single-pair cases. When comparing for instance again the NGGM and CAI11 instrument scenarios, the relative performance jump is much smaller compared to the product only single-pair jump. The same can be observed for CAI11 and CAI12. Since the performance of these instruments differs rather strongly in the low frequencies (<0.01 Hz) but not so in the high frequencies (>0.01 Hz) it is suspected that for double-pair scenarios the instrument performance in the longer wavelengths is of less importance than in case of single-pair scenarios. Thus, to proof this behavior, also for the double-pair scenarios, additional simulations with instrument noises just differing in the lower or higher frequencies have been performed (same as for single-pair). These simulations confirmed the smaller impact of the instrument performance in the lower frequencies for double-pair scenarios and indicated a rather increased sensitivity toward the higher frequencies compared to the single-pair scenarios.

It is supposed that the high sensitivity toward lower frequencies within (polar) single-pair scenarios is induced by the decreased stability of the gravity field inversion (through unconstrained least-squares adjustment) in case of unidirectional observations and no ground track crossings (except on the poles). In contrast, the second inclined pair in the double-pair scenarios introduces two additional observation directions (one for ascending and descending overflights) and ground track crossings (with itself and the polar pair). It is very intuitive that these advantages help to intrinsically mitigate long-wavelength drifts of the instruments (i.e., a higher instrument noise in the low frequencies). Due to the higher sensitivity of single-pair scenarios to the low frequencies of the accelerometer, CAI instruments may be particularly helpful here: Figure 3 highlights the performance differences between product-only single-pair scenarios NGGM and CAI11, which are mainly driven by the improved accelerometer performance in the long wavelengths (cf. Figure 1b). The improvement is particularly visible in the sectorial region (i.e., toward higher orders, cf. Figures 3a and 3c), which translates to a reduction of the striping patterns in the spatial plots (see Figures 3b and 3d).

Full-noise, single-pair. In contrast to the product-only scenarios, the full-noise scenarios include temporal aliasing as additional error source (through inclusion of time-variable gravity in the forward modeling). Hence, one may not expect the same direct scaling with the instrument noise level as in case of product-only. When comparing full-noise degree errors (cf. Figure 1b) to the product-only errors (Figure 1a) it is visible that all product-only retrieval errors (except single-pair GRACE-FO) are one or more orders of magnitude lower than the corresponding full-noise errors. This implicates that the retrieval error of all full-noise instrument scenarios (except GRACE-FO) is strongly dominated by temporal aliasing, which is why the actual noise level of the

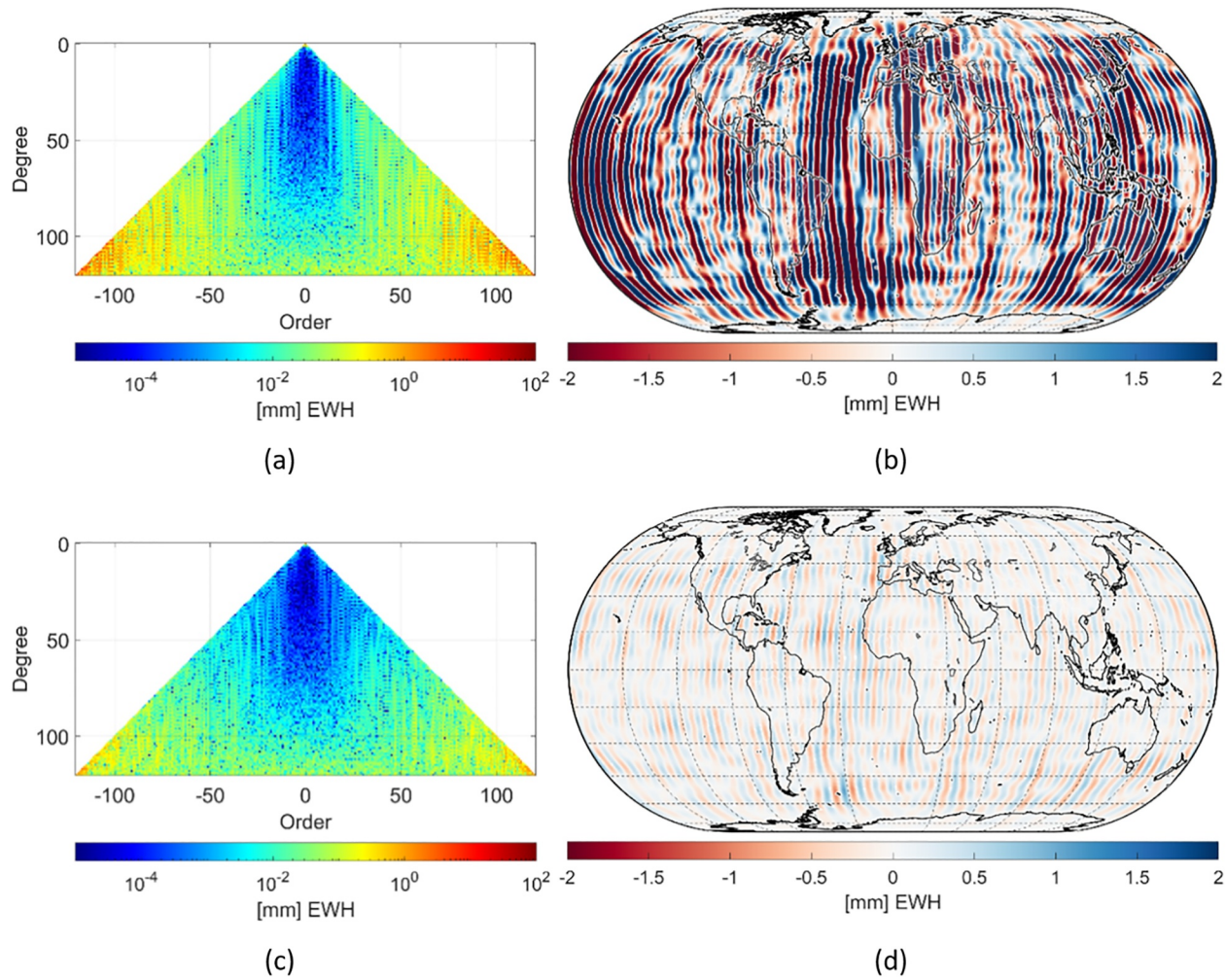

Figure 3. Coefficient triangles and corresponding spatial distribution of the errors of the product-only single-pair scenarios NGGM and CAI11 in terms of equivalent water heights. In the coefficient triangles, negative orders represent SH sine coefficients and positive orders cosine coefficients. (a) Coefficient triangle of the empirical errors of NGGM. (b) Spatial error distribution of NGGM. (c) Coefficient triangle of the empirical errors of CAI11. (d) Spatial error distribution of CAI11.

appropriate instrument is practically of no importance in case of full-noise (if equal or better than GRACE-FO). However, even if the actual instrument noise level is not relevant, the retrieval errors between the full-noise single-pair scenarios still differ. This is explained by the different shapes of the instrument ASDs since the ASD shape eventually interacts (positively or negatively) with the time-variable gravity signal within the gravity field retrieval (through a different weighting of the observations). Obviously, a steep slope in the low frequencies (resp. a dominant low frequency noise) shows the least favorable interaction with temporal aliasing in case of single-pair scenarios, since the NGGM instrument characteristics results in the worst full-noise retrieval error (NGGM noise has the steepest low frequency slope, cf. Figure 1b). In general, it seems that the lower the long-wavelength noise contribution in the instrument noise, the smaller the full-noise single-pair retrieval error (cf. Figure 1b solid lines and Figure 2b). Though, the overall achievable performance gain is very limited and even a scenario without instrument errors (cf. Figure 1b, orange dashed-dotted line) is bound by the same temporal aliasing barrier.

Full-noise, double-pair. In case of full-noise double-pair scenarios, the gravity field retrieval error of all instrument scenarios (even GRACE-FO) is strongly limited (by one or more orders of magnitude) by temporal aliasing (cf. Figure 1b dashed lines, similar to full-noise single-pair). However, in contrast to full-noise single-pair, the retrieval errors of all full-noise double-pair instrument scenarios are practically identical. This widely

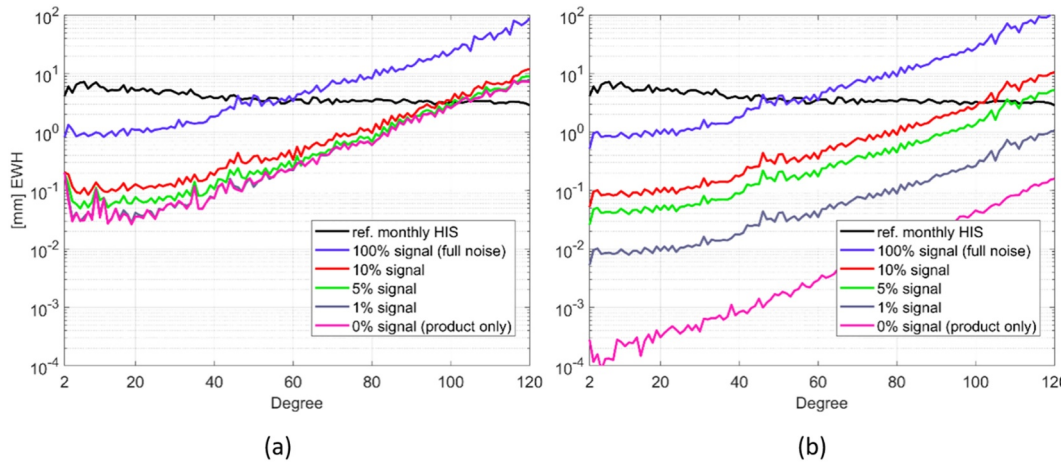

Figure 4. Degree errors in terms of equivalent water heights for simulations of double-pair instrument scenarios GRACE-FO (a) and CAI12 (b) with reduced time-variable input signal. The black curve shows the monthly reference mean signal (ESM components HIS + AO de-aliasing errors). Colored curves correspond to the retrieval errors at specific attenuation levels (of the time-variable components in the forward modeling, see legend).

agrees with the insights from the product-only scenarios, where the double-pair scenarios are also less influenced by the long-wavelength behavior of the instruments compared to the single-pair scenario.

For full-noise, it is assumed that the explanation for the sensitivity to the long-wavelength instrument behavior of single-pair scenarios is also related to the explanation given for the product-only scenarios: due to the decreased stability of the gravity field recovery in case of single-pair scenarios, it can be assumed that the individual weight of certain observations becomes stronger resp. weaker. Since an optimal time-averaging is generally obtained by equally weighting all observations (assuming an equally sampling in time) it is supposed that a stronger individual weighting (and also stronger correlations between observations) hampers the averaging process, thus, resulting in stronger temporal aliasing.

3.3. SST Simulations With Reduced Time-Variable Input Signal

As shown in the previous section, in case of full-noise, temporal aliasing significantly superimposes the instrument errors for all investigated scenarios. While a double-pair constellation helps to mitigate temporal aliasing to some extent (see Figure 2b), it still poses the dominant error source even there. To quantify the level to which temporal aliasing needs to be reduced that the instrument noise becomes relevant again, simulations with reduced time-variable gravity signal in the forward modeling are performed (by simply applying an attenuation factor to all time-variable components). Figure 4 shows the results of this test by comparing the worst-performing instrument scenario (GRACE-FO, Figure 4a) against the best-performing (CAI12, Figure 4b): it can be seen that, even in case of GRACE-FO instrument noise, temporal aliasing needs to be reduced to less than 10% before the sensor noise starts to contribute to the resulting retrieval error. In case of CAI12, even at 1% time-variable signal strength, temporal aliasing is still strongly dominating and the signal needs to be further reduced to less than 0.1% to discern the impact of the sensor noise.

Since no relevant performance differences are visible between the different full-noise instrument scenarios (due to temporal aliasing), further investigations of the benefits to the users (see Section 5) would also be futile. Hence, to still allow a further reasonable investigation of the potential benefits of improved instruments, it needs to be assumed that temporal aliasing could be reduced/eliminated by some means. Since the actual treatment of temporal aliasing would require additional sophisticated studies (e.g., of larger constellations, better de-aliasing and/or stochastic modeling), which cannot be covered by this contribution, achieving the product-only performance (see Figure 2b) is simply assumed for further studies on the benefit. For these studies (cf. Section 5), dedicated long-term product-only simulations (for the whole year 2002) have been performed for single- and double-pair constellations using a 7-day retrieval period; the weekly single-pair solutions are only calculated up to d/o 100 (instead of the default d/o 120) due to the limited ground-track coverage available after 1 week of accumulation time.

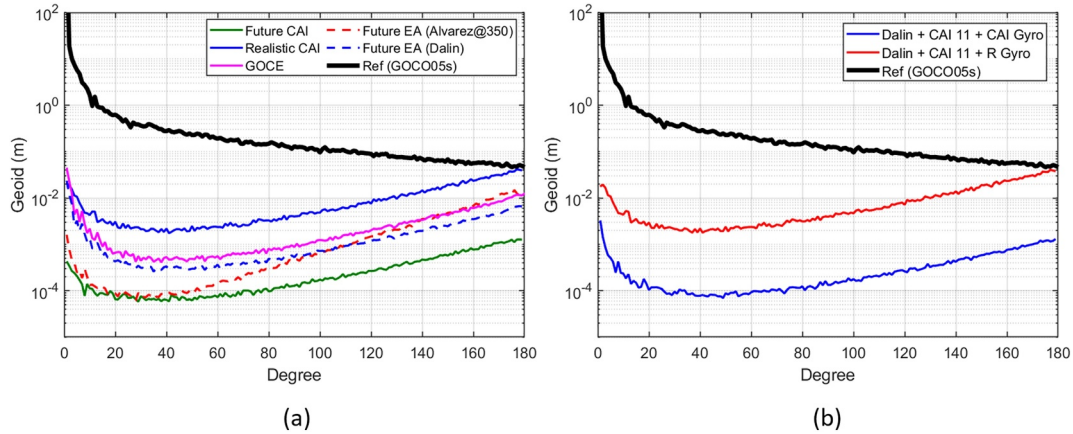

Figure 5. (a) Comparison between Realistic CAI, Future CAI, and Future electrostatic accelerometer instrument classes in terms of geoid (i.e., height anomaly) determination. (b) Impact of different gyroscopes (realistic vs. future).

4. SGG Simulations and Results

This section covers the setup and evaluation of the performed SGG simulation scenarios. In Section 4.1, we will describe the simulation setup and parameters, followed by the presentation and interpretation of the main results in Section 4.2. Additionally, we will delve into a detailed discussion on the retrieval of time-variable gravity signals.

4.1. SGG Simulator Setup

Simulation parameters/orbits. The simulation spanned a 2-month period, with data collected at 5-s intervals. To ensure a meaningful comparison between our findings and the GOCE mission (which serves as the reference for gradiometry) a GOCE-like orbit (96.7° inclination, 250 km altitude) was adopted, although a full polar orbit would be more favorable for gravity field recovery. Since all results are hence affected by the polar gap problem (i.e., an unresolvable zonal wedge in the SH coefficient triangle), the shown degree errors (Figures 5–7) are specifically tuned to mitigate it (by excluding these near zonal coefficients, see Sneeuw, 2000).

Forward modeling. The closed loop simulation utilized the GOCO05s model as the reference for the Earth's gravity field (EGM). In order to incorporate time variability into the gradiometry concept, non-tidal time-variable gravity components HIS from the ESA ESM is introduced in the forward modeling process, which represents the simulation of the true world. Both, the static and time-variable components of the gravity field are extended up to the spherical harmonic degree and order of 180 in the forward modeling.

Backward modeling. Similar to SST, for simulating the SGG concept, we also employ a common least-squares adjustment approach to recover the gravity field through a static SH parametrization. In the functional model, all three main diagonal components of the gravity gradient tensor are used according to the CAI gradiometer setup described in Section 2.3. As an advantage of least-squares adjustment, a rigorous error propagation of the instrument noise to the gravity field solution is possible, which enables an additional validation of the obtained empirical errors (by comparing to the formal errors). The formal errors of all results shown in Section 4.2 are in good agreement with the depicted empirical errors (cf. Figures 5–7).

4.2. SGG Simulation Results

Static gravity field retrieval. Utilizing the simulation setup described in Section 4.1, a comparative analysis between realistic and future scenarios has been conducted. Figure 5a presents the results for the scenarios defined in Section 2.3 (see Table 2). Figure 5b specifically highlights the impact of a CAI-based gyroscope compared to a realistic "external" gyroscope.

The realistic CAI cases, which are using different accelerometers reveal very similar results, which is attributed to the dominant error contribution of the realistic gyroscope in this category: since the error contribution of the

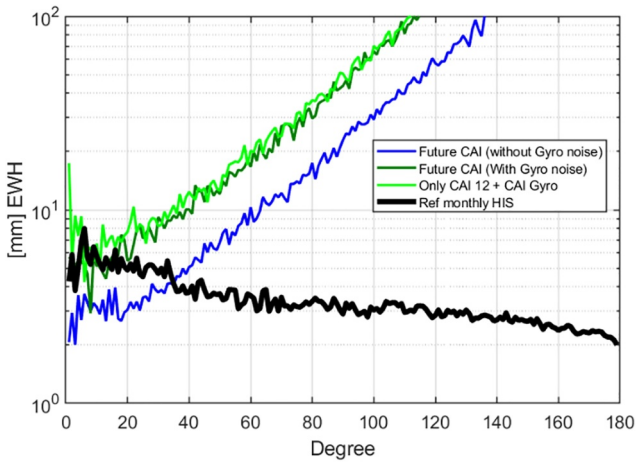

Figure 6. Time-variable gravity field retrieval with the satellite gravity gradiometry concept in terms of equivalent water heights.

gyroscope is dominating, the variations of the accelerometer noise level do not propagate to the gravity field retrieval error. Hence, only one representative curve is shown in Figure 5a. In contrast, the future CAI scenarios achieve a significant improvement in comparison to the realistic CAI class, reaching almost two orders of magnitude. Figure 5b underlines that these improvements can mainly be contributed to the improved gyroscope performance used in the future CAI scenarios.

All realistic and future scenarios are shown in relation to the GOCE mission, as depicted in Figure 5a. The GOCE curve corresponds to the analysis of 2 months of GOCE data (Pail et al., 2011). The realistic classes yield inferior results compared to the GOCE mission, primarily due to the large noise level of the "external" attitude data. In contrast, the future classes exhibit a noteworthy improvement surpassing the GOCE results by more than one order of magnitude.

To highlight the explicit benefit of future CAI accelerometers in comparison to future electrostatic accelerometers, Figure 5a also shows the results when only using a future electrostatic instrument without a CAI hybridization: the Dalin EA has an instrument ASD, which is very similar to the GOCE accelerometer with a slightly improved magnitude. Hence, also the gravity field retrieval errors of the Dalin and GOCE instrument scenarios are very similar and dominated by the long-wavelength instabilities of these electrostatic instruments (which obviously impact the gravity field over the whole spectrum). In contrast, the Alvarez@350 EA yields superior results in the low-frequency domain (similar to CAI instruments) but performs worse in the high-frequency domain due to the capacitive sensing characteristics of the accelerometer. This behavior is directly reflected in the gravity field retrieval performance where the Alvarez@350 EA can reach the (future) CAI error level in the low d/o but deteriorates toward the higher d/o (where the performance gets even worse than GOCE).

Time-variable gravity field retrieval. For studying the feasibility of time-variable gravity field retrieval with future SGG missions, three instrument scenarios are selected: (a) future CAI (without Gyro noise), (b) future CAI (with Gyro noise), and (c) only CAI 12 + CAI Gyro. Scenario (a) where the gyroscope noise is excluded is introduced to illustrate the specific impact of the gyroscope on the time-variable gravity field retrieval.

Figure 6 presents the related simulation results. The comparison of scenarios (a) and (b) highlights the significant impact of the gyroscope noise: in absence of attitude noise, temporal variations can be observed up to a spatial resolution of d/o 35. However, in presence of gyroscope noise the retrieval of time-variable gravity is almost impossible.

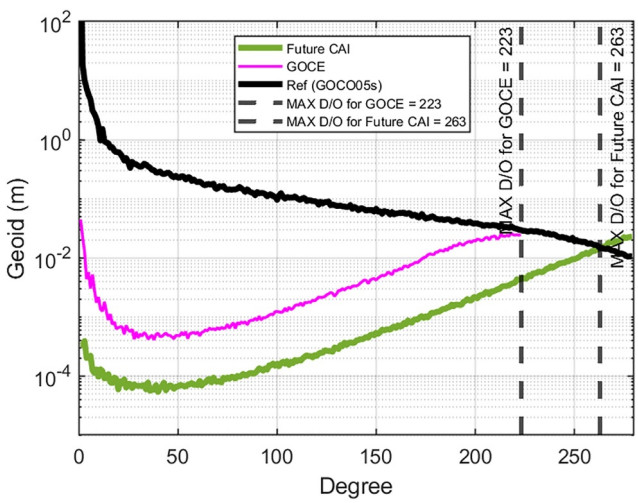

Figure 7. Maximum recoverable d/o with the future CAI satellite gravity gradiometry scenarios in comparison to GOCE.

Achievable spatial resolution. By reducing the (static) gravity field retrieval error, also higher maximum d/o become observable (since the signal-to-noise ratio remains above one for these higher d/o). Eventually, this means that also the achievable spatial resolution can be increased, as a maximum SH degree l_{max} can be related to a minimum spatial wavelength (spherical distance) d_{min} by $\sim 6{,}371[\mathrm{km}]\pi/l_{max}$. Figure 7 illustrates the improvement of the future CAI scenario over GOCE for a two-monthly retrieval period: the future CAI scenario can increase the maximum d/o to 263 (corresponding to a spatial resolution of ~76[km]) in comparison to a maximum d/o of 223 (~90[km]) achievable by the GOCE scenario.

5. Benefits on Hydrological Use Cases

The purpose of this section is to discuss the potential of the proposed mission scenarios for scientific and service applications, in particular in the field of hydrology. Terrestrial water storage (TWS) is mainly composed of groundwater, snow, ice, soil water, and of surface water in rivers, wetlands, natural lakes and man-made reservoirs (Güntner et al., 2007). In its capacity to expose long-term impacts on the global water cycle the variable "TWS

Table 3
Degree and Order (d/o) Where the Mean Weekly Retrieval Error of the Different Instrument Scenarios Exceeds the Mean Signal of the HIS Reference

Scenario	Cut-off polar pair constellation	Cut-off double pair constellation
GRACE	42	92
NGGM	73	120
CAI11	100	120
CAI12	100	120

Note. This d/o was used for each scenario as the cutoff for synthesizing the simulation results to the 1° degree global TWS grid.

anomalies" has been defined an essential climate variable (ECV) by the Global Climate Observing System (GCOS, https://gcos.wmo.int/en/essential-climate-variables/tws). Satellite gravimetry is the only available technology to measure this ECV on a global scale. As derivate from TWS further ECVs can be monitored, as demonstrated for the ECV product "groundwater storage change" by the project Global Gravity-based Groundwater Product (G3P, Güntner et al., 2023). In the following, we want to address the question: Do hydrological application cases benefit from quantum technology on future gravimetry missions?

5.1. Input Data

From the simulated (product-only) time-variable gravity fields presented in Section 3.3, global time series of TWS were derived by synthesizing the simulation results in terms of EWH to regular 1° grids of 7-day mean TWS anomalies. The (product-only) instrument scenarios were resolved to the d/o where their mean (weekly) retrieval error exceeded the mean signal of the HIS reference (see Table 3).

As a basis for the comparison, TWS anomaly time series from a real-world model were used, that is, the HIS-component (hydrology, ice, solid earth) of the ESA ESM. Instrument scenarios were simulated for the year 2002. The HIS reference was provided for the period of 1995–2006 (12 years) and resolved up to d/o 120. When introducing the reference up to d/o 120, omission errors induced by the limited spatial resolution are minimized, at least for the double-pair scenarios (see Table 3). Furthermore, it is assumed that the signal separation between the ESM components AO and HIS can be performed perfectly. Hence, in these scenarios, temporal aliasing, omission errors, and signal separation errors are neglected, which allows to focus entirely on the instrument errors. This has to be kept in mind when interpreting the following evaluations.

We removed the 12-year linear trend at the grid cell scale to minimize possibly disturbing effects of long-term processes such as glacier melt or man-made groundwater depletion on the analysis of the short-term hydrometeorological phenomena considered here. The evaluation of hydrological application cases was focused on 474 of the 520 world's largest river basins from the data set "Major River Basins of the World" of the Global Runoff Data Center (GRDC, 2020). 46 basins had to be discarded since their geometry did not allow for an assessment with the 1° grid resolution.

5.2. Method

Area averages and RMSD calculation. Based on the basins we calculated latitude-dependent area averages for all 1° grid data sets. From these the root mean squared deviation (RMSD) between the individual instrument scenarios and the HIS reference were calculated for 2002 as an empirical estimate of the error of the instrument scenarios. For comparison of the scenarios the RMSD values of the 474 river basins were scatter plotted against their basin area and the performance of the instrument scenarios were compared.

Detection of hydrological extremes. To evaluate the individual instrument scenarios with respect to their potential to detect hydrological extremes, the instrument scenarios were analyzed for time steps in which certain thresholds that define wet or dry TWS extremes were crossed. The thresholds for wet (99th, 98th, and 95th percentile) and dry extremes (1st, 2nd, and 5th percentile) were derived from percentiles of the 12-year HIS reference (1995–2006). The 1-year instrument scenario simulations were then compared to those thresholds to check if an extreme was detected by the scenario.

The following features were assessed for scenario comparison:

I. In how many of the 474 basins an extreme was correctly detected.

In these correctly identified basins.

II. How many peaks were detected in the correct 7-day time step (*CP*) and
III. How many peaks were detected in the wrong time step (*IP*).
IV. The mean deviation in TWS anomalies of the correctly detected peaks between scenario and reference.

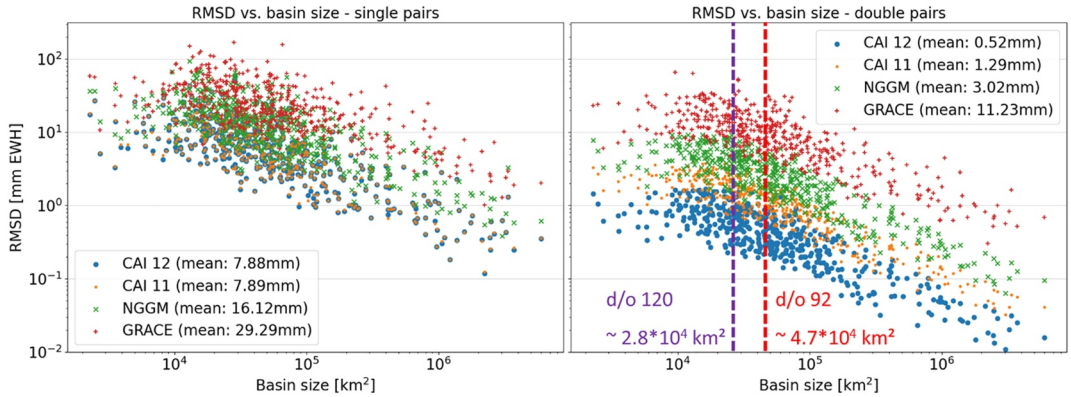

Figure 8. Root mean squared deviation values of the four instrument scenarios as single pair constellation (left) and double pair constellation (right). Vertical lines in the right plot indicate the cut-offs and the approximate spatial resolution that results from them, that is, the sizes of a basin that could reliably be assessed with the cut-off.

To fuse parameters II and III, we calculated a statistical score that benchmarks the capability of a scenario to correctly detect peaks:

$$\text{Score} = \frac{CP - IP}{N_{ref}} \tag{9}$$

with CP the correct peaks, IP the incorrect peaks, and N_{ref} the total number of peaks in reference.

Furthermore, it was evaluated:

V. How often a basin was registered as having an extreme when in the reference was having none at all and
VI. How many peaks crossed the threshold in that particular year. The latter has proven to be a good indicator for the noisiness of a time series.

Please note that we define the term peak as a time step where TWS crosses the defined threshold. In case of the dry extremes, this means a negative peak in the anomalies (a very low TWS value).

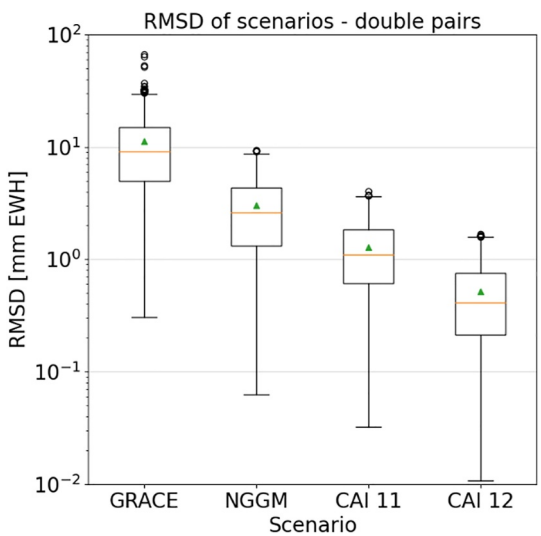

Figure 9. Box plot for the four instrument scenarios in double pair constellation. The plot only includes the 237 basins that are on the right of the red line in Figure 8, that is, larger than about 47,000 km^2 (d/o 92).

5.3. Results

Area averages and RMSD calculation. The RMSD values of the single-pair constellations differ only slightly among them and are not suited to differentiate between the error properties of the four instrument scenarios (compare Figure 8). However, we have to point out the different cut-offs of the individual instrument scenarios, which might lead to a dominance of the omission error (see Table 3).

In double-pair constellation, the scenarios are well distinguishable. The differences between the scenarios spread across 1.5 orders of magnitude, with performance increase in the order from GRACE, over NGGM to CAI11 and CAI12. Furthermore, it is clear that there is a performance increase with basin size, which is probably linked to the spherical-harmonic cut-off degree and the generally limited spatial resolution of the method (compare Table 3).

As mentioned above, with the scenarios with resolution below d/o 120, there remains a possibility that the omission error is the dominating factor. This does not apply to CAI12, CAI11, and NGGM, which have been resolved up to d/o 120. Considering the double pair constellations in more detail (Figure 8) only GRACE remains below that resolution. Accordingly, the box plot in Figure 9 focuses on the 237 basins that can be assessed by each of the four scenarios in a similar way. However, the above observed pattern remains, and

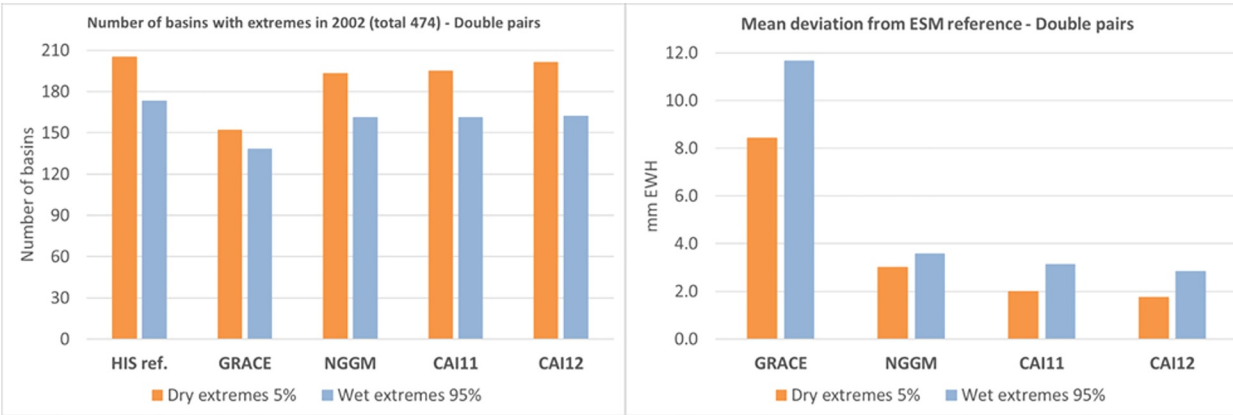

Figure 10. Number of basins with extremes in the year 2002 (parameter I, left) and mean deviation of the extremes from the ESM reference (parameter IV, right). Total number of basins assessed in the study is 474.

we see that the quantum-based accelerometers outperform the electrostatic accelerometers by about 1–1.5 orders of magnitude. In the case of CAI12 the difference is significant Figure 10.

Looking at Figure 8 from another perspective, we can say that the scenarios NGGM, CAI11, and CAI12 in comparison to GRACE would allow for an additional assessment of 91 basins with sizes between 28,000 and 47,000 km^2. This is an increase of 38.4%.

Detection of hydrological extremes. As a first outcome, it became apparent that patterns in the results for the different percentiles are similar and deviations from the ESM reference for each scenario remain stable across percentiles. For the sake of briefness, we will hence focus on the 5th and 95th percentiles (Table 4). Tables A1 and A2 with full results can be found in the appendix.

The results show that the general pattern of double pairs outperforming the single pairs persists for parameters I and III to VI. Only for parameter II, results are rather similar across constellations and instrument scenarios.

The detection rate of extremes (parameter I) increases slightly in the same order as in the results for the RMSD values, that is, from GRACE over NGGM to the two CAI scenarios (Figure 11). Again it should be noted that

Table 4
Summary Statistics for the Hydrological Extremes

	Dry extremes 5%								Wet extremes 95%							
	I	I	II (CP)	III (IP)	Score	IV	V	VI	I	I	II (CP)	III (IP)	Score	IV	V	VI
	n	%/%*				mm			N	%/%*				mm		
ESM	205	43.2/-	7.1	-	1	-	-	-	173	36.5/-	5.9	-	1	-	-	-
Single pair constellations																
GRACE	79	16.7/38.5	5.5	7.9	−0.33	13.6	70	8.4	85	17.9/49.1	4.8	4	−0.06	20.3	39	4.3
NGGM	120	25.3/58.5	5.9	5.8	−0.21	9.1	59	6.9	128	27/74	5.4	2.4	0.34	13.7	31	2.9
CAI11	161	34/78.5	6.1	4.1	0.24	7.2	38	5.7	146	30.8/71.2	5.6	1.9	0.56	8.2	14	2.4
CAI12	160	33.8/78	6.2	4.2	0.24	7.3	37	5.7	144	30.4/83.2	5.7	1.8	0.56	8.3	13	2.6
Double pair constellations																
GRACE	152	32.1/74.1	5.9	5.4	0.14	8.4	55	7.3	138	29.1/79.8	5.6	2.3	0.48	11.6	31	3
NGGM	193	40.7/94.1	6.4	2.9	0.49	3.0	30	3.5	161	34/93.1	5.6	1.3	0.72	3.6	11	1.4
CAI11	195	41.1/95.1	6.5	1.9	0.7	2.0	15	2.1	161	34/93.1	5.8	1.1	0.77	3.1	7	1
CAI12	201	42.4/98	6.6	1.5	0.7	1.7	6	1.2	162	34.2/93.6	5.8	1.1	0.8	2.8	6	1.2

Note. For explanation of parameters I to VI and the score, see the main text at the beginning of this chapter. Parameter I is given as number (n) and as percentage in relation to the total number of 474 basins (%) and to the number of basins with an extreme in the ESM (%*).

10.1029/2024EA003630

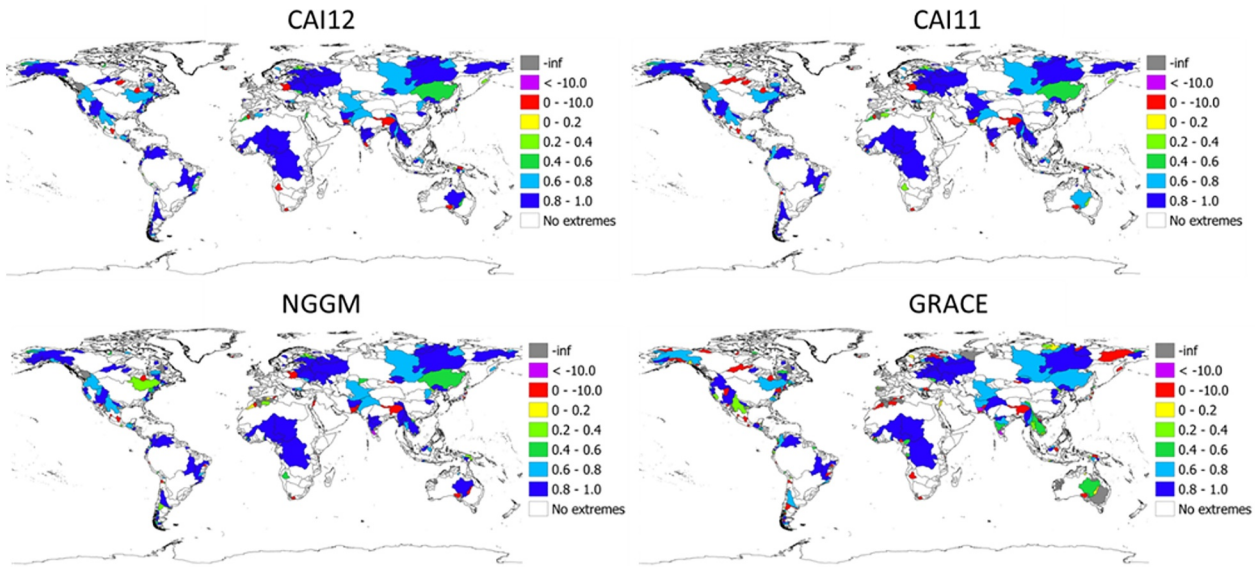

Figure 11. Score (according to Equation 9) for detecting dry extremes (5% threshold) in 2002, for the difference scenarios in the double pair constellations.

different cut-offs have been used for the different scenarios (Table 3). As it is likely that results for the single pair constellations are mainly influenced by the omission error, we will focus on the double pair constellations in the following. Here it becomes apparent that the scenarios with equal cut-offs, that is, NGGM, CAI11 and CAI12, have very similar detection rates and hence parameter I is not well suited to assess performance. To a slightly lesser extent, this is also the case for parameter IV.

The order of performance of the different scenarios persists when looking at the detection of hydrological extremes, described by parameters II and III in Table 4. For both dry and wet extremes, the number of correctly detected peaks (CP) in basins that had extremes in the study year 2002 increases while the number of incorrect peaks (IP) decreases. The performance differences between the scenarios are a bit more pronounced in the single pair constellations and for the IP.

A combination of parameters II and III is the score presented in Table 4 and plotted as maps of the basins in Figure 11, for the example of the dry extremes and the double pair constellation. The order of performance also persists here, with poorer performance of the GRACE scenario, and again a bit more pronounced for the single pair constellations (not shown). The patterns show no clear geographical distribution. However, they indicate that smaller river basins, often located in coastal regions, tend to have a lower performance, illustrated by reddish colors or dark gray (the latter marks basins that have extremes in the scenario but none in the reference data). As the signal-to-noise ratio tends to increase when averaging over larger areas, this behavior is to be expected.

While the above results show rather moderate differences between the scenarios, the differences become much clearer when looking at the number of false positive basins (parameter V in Table 4) and the number of peaks in the false positive basins (parameter VI) (Figure 12). The latter is a good measure of the noisiness of a time series. For the wet and dry extremes, we see the former pattern of performance increase between the scenarios. But especially for the dry extremes, we see a clear improvement with a lower number of false positive basins toward the quantum-based scenarios that previously were not so clearly discernible from the NGGM performance. However, it is remarkable that for the wet extremes there is virtually no difference between the CAI11 and the CAI12 scenarios. Furthermore, it is remarkable that the detection of wet extremes tends to produce less false positives than the dry extremes. The number of false positive peaks seems to closely correlate with the number of false positive basins, which indicates that lower noisiness of a time series reduces errors in extreme detection.

Discussion. The definition of requirements for satellite gravimetry missions in respect to a desired performance for hydrological application cases is very complex and can only be achieved in close exchange with all involved scientific disciplines. A comprehensive result of such discussions are the current MAGIC mission requirements

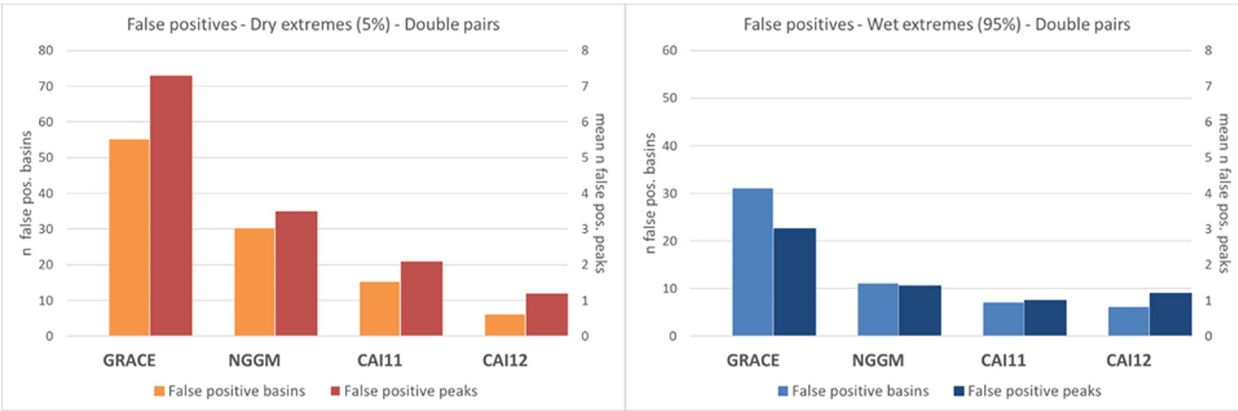

Figure 12. Number of basins where extremes in 2002 were seen in the scenarios when while there was no extreme in the ESM reference ("false positive basin"), and the mean number of peaks in those basins ("false positive peaks") for the dry (left) and the wet extremes (right) for the double pair constellations. Please note the two differently scaled ordinates.

(Haagmans and Tsaoussi, 2020) based on Pail et al. (2015). This mission requirement document (MRD) gives a threshold requirement for accuracy of 60 mm EWH and a target requirement for accuracy of 6 mm EWH for weekly TWS data at the spatial resolution we are looking at in this study, that is, 166–217 km (d/o 120 and 92) in the case of double pair constellations.

To achieve the desired comparability of scenarios, we made a series of far-reaching assumptions in terms of background models and omission errors. Accordingly, we were looking at somewhat unrealistically optimized simulations. The errors of the simulation, above expressed as RMSD values, hence widely ranged better than the target requirements from the MAGIC MRD. Only some small basins in the GRACE scenario tested could not meet the threshold mission requirements. Considering the accuracy of the detection of hydrological extremes, all single pair scenarios and the GRACE double pair scenarios are worse than the target requirement of the MAGIC MRD with accuracies going up to 20 mm, however still better than the threshold requirement. NGGM, CAI11, and CAI12 as double pairs all perform better than the target requirement of 6 mm.

Another clear result is the overall superior performance of the larger constellation. With the better signal-to-noise ratio of the double pair constellation, especially for NGGM, CAI11, and CAI12, a significantly larger number of small basins could be assessed. Accordingly, we support the planned double pair constellation of the MAGIC MRD.

To answer our initially posed question, if hydrological application cases benefit from quantum technology on future gravimetry missions, we can summarize that in parts the quantum-based technologies delivered better results than the electrostatic accelerometers, especially than GRACE. While major improvements are seen by adding a second satellite pair, additional quantum-based scenarios in comparison to the MAGIC double pair, are seen by a lower number of false positives for the detection of hydrological extremes, for example, Additionally, it has to be stated that the CAI11 scenario, which in general is considered to be more realistic from a technological perspective than the CAI12 scenario, widely performed as fine as the latter.

6. Conclusions

In this contribution, the impact of future (quantum) accelerometers on the SST and SGG mission concept has been investigated. For SST, this impact can be quantified on different processing levels: (a) on the in situ observation level, (b) on the level of global gravity field models, and (c) on user product level (e.g., TWS grids).

The benefit on (a) the in situ observations can directly be inferred by inspecting the SST instrument product noise (see Section 2.2) and is also reflected in the product-only gravity field solution (Section 3). Obviously, future instrument scenarios enable smaller observation errors, and, thus, allow to observe the gravity field more precisely. However, one has to keep in mind that, in case of SST, the product noise is a combination of the accelerometer noise and the noise of the ranging instrument. Consequently, for improving the observation noise, also improved ranging instruments need to be considered. When inspecting the combined (product) noise of the best-

performing instrument scenario (CAI12), it is seen that it is completely dominated by the noise of the ranging instrument. In this case, an additional improvement of the accelerometer would not reduce the final observation errors any further.

When deriving (b) global gravity field models from in situ observations, certain accumulation times need to be considered to achieve the necessary global observation coverage through the satellites' ground tracks. For single-pair and double-pair missions, an accumulation time (retrieval period) of several days (e.g., 1 week) is usually required (depending on the spatial target resolution and available orbital sub-cycles). This accumulation time defines basically the maximum achievable temporal sampling rate. From the time-variable background models (ESM, ocean tides) it is known that they contain significant signal content up to half-daily frequencies and beyond (e.g., see Daras & Pail, 2017). Eventually, this implies that significant temporal aliasing is introduced when deriving global gravity fields from single- and double-pair SST missions. In fact, the errors induced by temporal aliasing are in all investigated instruments scenarios much larger than the errors induced by the instruments (see Section 3.2). Hence, for small constellations, the benefit of improved (accelerometer) instruments is very limited on thereof derived global gravity field models. To reduce the primary error source (i.e., temporal aliasing), larger constellations are necessary, which enable a higher spatio-temporal resolution. Temporal aliasing could theoretically also be mitigated by improving the background/de-aliasing models. Though, the applied background models would need to improve by at least a factor of 10 (cf. Section 3.3) which seems not achievable within the near future.

As hydrological users are only interested in the components of the gravity signal that relate to hydrologically induced, that is, TWS changes, processing requires signal separation. The task of signal separation can inherently not be solved through gravity observations alone and requires additional information, for example, from models and/or complementary data sets. The accuracy of this information poses an additional error source which, eventually, supersedes the instrument errors. Hence, before improved technologies as discussed in this study may have a beneficial impact on hydrological user applications, further progress in processing has to be made. This is illustrated by the fact that only after ignoring the effect of temporal aliasing, the impact of better instruments on hydrological applications could be quantified (see Section 5). Nevertheless, adding a second SST pair results in the largest performance gain for hydrological applications.

Finally, for SST, it can be stated that instrument errors reflect one of the primary error sources. However, the errors induced through temporal aliasing are currently significantly more prominent (when deriving global gravity field models). Thus, from a general perspective, reducing temporal aliasing is at the moment a more important task than further reducing the instrument noise level. Considering the investigated single- and double-pair SST mission scenarios, a lower instrument noise could only be fully exploited by the users if they would be able to work directly with in situ SST observations (since temporal aliasing would be completely mitigated then). We emphasize that these findings are valid for all future instrument scenarios and are not peculiar to CAI.

Similar to SST, also for SGG, it could be shown that improved accelerometers/gradiometers allow to observe the gravity observable (i.e., the gradient) more precisely (see Section 4). Though, if not the complete gradient tensor is observable (since this would basically require six 3D accelerometers), the satellite's attitude needs to be determined with a very high accuracy through complementary instruments. Currently, the available attitude sensors for this task are not sensitive enough to exploit the full performance gain achievable with future gradiometers. On the other hand, even if the attitude problem could be solved somehow, the projected sensitivity of future (CAI) gradiometers is still not high enough to compete with the performance of SST missions for time-variable gravity field recovery. However, it could be shown that CAI SGG instruments can deliver a lower noise than the GOCE gradiometer, which, consequently, would allow to derive higher-resolution static gravity field models and with higher accuracy than currently available.

Appendix A

Table A1
Count (n) of Basins That Contained a Dry Extreme in 2002 and Their Ratio (A) of the Total Number of Basins (474). B is the Deviation of the Detected Extreme From the Extreme in the ESM Reference

	Dry extremes								
	1%			2%			5%		
	n	A %	B mm	n	A %	B mm	n	A %	B mm
ESM	73	15.4		110	23.2		205	43.2	
Single pair constellations									
GRACE	19	4	10.3	36	7.6	10.3	79	16.7	13.6
NGGM	31	6.5	3.5	55	11.6	5.4	120	25.3	9.1
CAI11	48	10.1	5.6	71	15	6.2	161	34	7.2
CAI12	46	9.7	5.5	72	15.2	6.1	160	33.8	7.3
Double pair constellations									
GRACE	37	7.8	5.3	68	14.3	6.0	152	32.1	8.4
NGGM	60	12.7	2.3	92	19.4	2.4	193	40.7	3.0
CAI11	66	13.9	1.4	96	20.3	1.6	195	41.1	2.0
CAI12	65	13.7	1.2	95	20	1.2	201	42.4	1.7

Table A2
Count (n) of Basins That Contained a Wet Extreme in 2002 and Their Ratio (A) of the Total Number of Basins (474). B is the Deviation of the Detected Extreme From the Extreme in the ESM Reference

	Wet extremes								
	99%			98%			95%		
	n	A %	B mm	n	A %	B mm	n	A %	B mm
ESM	62	13.1		93	19.6		173	36.5	
Single pair constellations									
GRACE	17	3.6	14.2	32	6.8	16.8	85	17.9	20.3
NGGM	34	7.2	9.5	57	12	10.6	128	27	13.7
CAI11	40	8.4	7.1	83	17.5	7.5	146	30.8	8.2
CAI12	41	8.6	7.3	82	17.3	7.3	144	30.4	8.3
Double pair constellations									
GRACE	34	7.2	9.1	71	15	9.9	138	29.1	11.6
NGGM	53	11.2	3.4	81	17.1	3.8	161	34	3.6
CAI11	55	11.6	2.8	84	17.7	3.0	161	34	3.1
CAI12	54	11.4	2.8	84	17.7	2.9	162	34.2	2.8

Data Availability Statement

Data associated with this manuscript can be found in the supplementary data repository (Zingerle et al., 2024). Simulation software cannot be shared due to intellectual property rights. However, the underlying methodology is published, and a corresponding reference is provided.

Acknowledgments
The investigations were supported by funding of the German Federal Ministry of Economic Affairs and Energy (BMWi), projects 50EE2220 (A/B/C). M.R. and J. M. acknowledge Deutsche Forschungsgemeinschaft (DFG)—TerraQ (Project-ID 434617780—SFB 1464) and German Aerospace Center (DLR)—Q-BAGS (Project-ID 50WM2181). Computations were carried out using resources of the Leibniz Supercomputing Centre (LRZ) and the cluster system at the Leibniz University of Hannover, Germany. Open Access funding enabled and organized by Projekt DEAL.

References

Abend, S., Gersemann, M., Schubert, C., Schlippert, D., Rasel, E. M., Zimmermann, M., et al. (2020). Atom interferometry and its applications. In E. M. Rasel & W. S. SchleichW (Eds.), *Proceedings of the international school of physics* (Vol. 197, pp. 345–392). https://doi.org/10.3254/978-1-61499-937-9-345

Abrykosov, P., Pail, R., Gruber, T., Zahzam, N., Bresson, A., Hardy, E., et al. (2019). Impact of a novel hybrid accelerometer on satellite gravimetry performance. *Advances in Space Research*, *63*(10), 3235–3248. https://doi.org/10.1016/j.asr.2019.01.034

Alvarez, A., Knudtson, A., Patel, U., Gleason, J., Hollis, H., Sanjuan, J., et al. (2022). A simplified gravitational reference sensor for satellite geodesy. *Journal of Geodynamics*, *96*(10), 70. https://doi.org/10.1007/s00190-022-01659-0

Armano, M., Audley, H., Baird, J., Binetruy, P., Born, M., Bortoluzzi, D., et al. (2018). Beyond the required LISA free-fall performance: New LISA pathfinder results down to 20 mHz. *Physical Review Letters*, *120*(6), 061101. https://doi.org/10.1103/physrevlett.120.061101

Cesare, S., Dionisio, S., Saponara, M., Bravo-Berguño, D., Massotti, L., da Encarnação, J. T., & Christophe, B. (2022). Drag and attitude control for the next generation gravity mission. *Remote Sensing*, *14*(12), 2916. https://doi.org/10.3390/rs14122916

Christophe, B., Boulanger, D., Foulon, B., Huynh, P. A., Lebat, V., Liorzou, F., & Perrot, E. (2015). A new generation of ultra-sensitive electrostatic accelerometers for GRACE Follow-on and towards the next generation gravity missions. *Acta Astronautica*, *117*, 1–7. https://doi.org/10.1016/j.actaastro.2015.06.021

Dalin, M., Lebat, V., Boulanger, D., Liorzou, F., Christophe, B., Rodrigues, M., & Huynh, P. A. (2020). ONERA accelerometers for future gravity mission. *EGU General Assembly 2020*. https://doi.org/10.5194/egusphere-egu2020-5721

Daras, I. (2016). Gravity Field Processing Towards Future LL-SST Satellite Missions, Deutsche Geodätische Kommission der Bayerischen Akademie der Wissenschaften, Reihe C. *Dissertationen, Heft*, *770*, 23–39.

Daras, I., March, G., Pail, R., Hughes, C. W., Braitenberg, C., Güntner, A., et al. (2024). Mass-change and Geosciences International Constellation (MAGIC) expected impact on science and applications. *Geophysical Journal International*, *236*(3), 1288–1308. https://doi.org/10.1093/gji/ggad472

Daras, I., & Pail, R. (2017). Treatment of temporal aliasing effects in the context of next generation satellite gravimetry missions. *J. Geophys. Res. (Solid Earth)*, *122*(9), 7343–7362. https://doi.org/10.1002/2017jb014250

Daras, I., Pail, R., Murböck, M., & Yi, W. (2015). Gravity field processing with enhanced numerical precision for LL-SST missions. *Journal of Geodynamics*, *89*(2), 99–110. https://doi.org/10.1007/s00190-014-0764-2

Dobslaw, H., Bergmann-Wolf, I., Dill, R., Forootan, E., Klemann, V., Kusche, J., & Sasgen, I. (2015). The updated ESA Earth System Model for future gravity mission simulation studies. *Journal of Geodynamics*, *89*(5), 505–513. https://doi.org/10.1007/s00190-014-0787-8

Douch, K., Wu, H., Schubert, C., Müller, J., & Pereira Dos Santos, F. (2018). Simulation-based evaluation of a cold atom interferometry gradiometer concept for gravity field recovery. *Advances in Space Research*, *61*(5), 1307–1323. https://doi.org/10.1016/j.asr.2017.12.005

Drinkwater, M. R., Floberghagen, R., Haagmans, R., Muzi, D., & Popescu, A. (2003). GOCE: ESA's first earth explorer core mission. In G. Beutler, M. R. Drinkwater, R. Rummel, & R. Von Steiger (Eds.), *Earth gravity field from space — from sensors to earth sciences*, *Space sciences series of ISSI* (Vol. 17, pp. 419–432). Springer. https://doi.org/10.1007/978-94-017-1333-7_36

Flechtner, F., Webb, F., & Watkins, M. (2017). Current status of the GRACE follow-on mission. *Geophysical Research Abstracts*, *19*. EGU 2017–4566, EGU General Assembly 2017.

Frommknecht, B., Oberndorfer, H., Flechtner, F., & Schmidt, R. (2003). Integrated sensor analysis for GRACE - development and validation. *Advances in Geosciences*, *1*, 57–63. https://doi.org/10.5194/adgeo-1-57-2003

GRDC. (2020). Major River basins of the world/global Runoff data Centre. *GRDC. 2nd, rev. ext. ed. Koblenz, Germany: Federal Institute of Hydrology (BfG)*.

Güntner, A., Sharifi, E., Behzadpour, S., Boergens, E., Dahle, C., Darbeheshti, N., et al. (2023). Global gravity-based groundwater product (G3P). V. 1.11. *GFZ Data Services*. https://doi.org/10.5880/G3P.2023.001

Güntner, A., Stuck, J., Werth, S., Döll, P., Verzano, K., & Merz, B. (2007). A global analysis of temporal and spatial variations in continental water storage. *Water Resources Research*, *43*(5), W05416. https://doi.org/10.1029/2006WR005247

R. Haagmans & L. Tsaoussi (Eds.) (2020). Next generation gravity mission as a mass-change and geosciences international constellation (MAGIC) mission requirements document. In *Earth and mission science division*. European Space Agency; NASA Earth Science Division. https://doi.org/10.5270/esa.nasa.magic-mrd.2020

Hauk, M., Wilms, J., Sulzbach, R., Panafidina, N., Hart-Davis, M., Dahle, C., et al. (2023). Satellite gravity field recovery using variance-covariance information from ocean tide models. *Earth and Space Science*, *10*(10), e2023EA003098. https://doi.org/10.1029/2023EA003098

Heller-Kaikov, B., Pail, R., & Daras, I. (2023). Mission design aspects for the mass change and geoscience international constellation (MAGIC). *Geophysical Journal International*, *235*(1), 718–735. https://doi.org/10.1093/gji/ggad266

Knabe, A. (2023). New concepts for gravity field recovery using satellites. PhD thesis. *Fachrichtung Geodäsie und Geoinformatik der Leibniz Universität Hannover*.

Knabe, A., Schilling, M., Wu, H., HosseiniArani, A., Müller, J., Beaufils, Q., & Pereira dos Santos, F. (2022). The benefit of accelerometers based on cold atom interferometry for future satellite gravity missions. In *International association of geodesy symposia*. Springer. https://doi.org/10.1007/1345_2022_151

Kornfeld, R. P., Arnold, B. W., Gross, M. A., Dahya, N. T., Klipstein, W. M., Gath, P. F., & Bettadpur, S. (2019). GRACE-FO: The gravity recovery and climate experiment follow-on mission. *Journal of Spacecraft and Rockets*, *56*(3), 931–951. https://doi.org/10.2514/1.a34326

Kupriyanov, A., Reis, A., Schilling, M., Müller, V., & Müller, J. (2024). Benefit of enhanced electrostatic and optical accelerometry for future gravimetry missions. *Advances in Space Research*, *73*(6), 3345–3362. https://doi.org/10.1016/j.asr.2023.12.067

Lenoir, B., Lévy, A., Foulon, B., Lamine, B., Christophe, B., & Reynaud, S. (2011). Electrostatic accelerometer with bias rejection for gravitation and Solar System physics. *Advances in Space Research*, *48*(7), 1248–1257. https://doi.org/10.1016/j.asr.2011.06.005

Lévèque, T., Fallet, C., Lefebve, J., Piquereau, A., Gauguet, A., Battelier, B., et al. (2022). Carioqa: Definition of a quantum pathfinder mission proceedings of international conference on space optics (ICSO) 2022; 3-7 October 2022; Dubrovnik; Croatia. https://doi.org/10.48550/arXiv.2211.01215. arXiv:2211.01215 [physics.atom-ph]

Mayer-Gürr, T. (2006). Gravitationsfeldbestimmung aus der Analyse kurzer Bahnbögen am Beispiel der Satellitenmissionen CHAMP und GRACE, Dissertation. *Rheinische Friedrich-Wilhelms-Universität Bonn*. https://nbn-resolving.org/urn:nbn:de:hbz:5N-09047

Mayer-Gürr, T., Pail, R., Fecher, R., & Gruber, T., & GOCO Team. (2015). *The combined satellite gravity field model GOCO05s*. European geosciences union general assembly.12364.

Meister, J., Bremer, S., HosseiniArani, A., Leipner, A., List, M., Müller, J., & Schilling, M. (2022). Reference mirror misalignment of cold atom interferometers on satellite-based gravimetry missions. 73rd international astronautical congress (IAC). *Proceedings, IAC-22, B1, IP*, *7*, x68955.

Müller, J., & Wu, H. (2020). Using quantum optical sensors for determining the Earth's gravity field from space. *Journal of Geodynamics*, *94*(8), 1–14. https://doi.org/10.1007/s00190-020-01401-8

Pail, R., Bruinsma, S., Migliaccio, F., Förste, C., Goiginger, H., Schuh, W. D., et al. (2011). First GOCE gravity field models derived by three different approaches. *Journal of Geodynamics*, *85*(11), 819–884. https://doi.org/10.1007/s00190-011-0467-x

Pail, R., Bingham, R., Braitenberg, C., Eicker, A., Horwath, M., Ivins, E., et al. (2015). Observing mass transport to understand global change and to benefit society: Science and user needs – An international multi-disciplinary initiative for IUGG. Heft 320, ISBN 978-3-7696-8599-2, München https://gfzpublic.gfz-potsdam.de/pubman/item/item_1354175,DeutscheGeodätischeKommissionderBayerischen AkademiederWissenschaften

Ray, R. (2008). *GOT4.7. Extension of Ray R (1999) A global ocean tide model from Topex/Poseidon altimetry GOT99.2*. NASA Tech Memo.209478.

Savcenko, R., & Bosch, W. (2012). *EOT11a - empirical ocean tide model from multi-mission satellite altimetry*. DGFI-Report No. 89.

Savoie, D., Altorio, M., Fang, B., Sidorenkov, L. A., Geiger, R., & Landragin, A. (2018). Interleaved atom interferometry for high-sensitivity inertial measurements. *Science Advances*, *4*(12), aau7948. https://doi.org/10.1126/sciadv.aau7948

Siemes, C. (2018). Improving GOCE cross-track gravity gradients. *Journal of Geodynamics*, *92*(1), 33–45. https://doi.org/10.1007/s00190-017-1042-x

Sneeuw, N. (2000). A semi-analytical approach to gravity field analysis from satellite observations. *Deutsche Geodaetische Kommission, Reihe C, Heft Nr*, *527*, 69–73.

Stummer, C., Fecher, T., & Pail, R. (2011). Alternative method for angular rate determination within the GOCE gradiometer processing. *Journal of Geodynamics*, *85*(9), 585–596. https://doi.org/10.1007/s00190-011-0461-3

Tapley, B. D., Bettadpur, S., Watkins, M., & Reigber, C. (2004). The gravity recovery and climate experiment experiment: Mission overview and early results. *Geophysical Research Letters*, *31*(9). https://doi.org/10.1029/2004gl019920

Touboul, P. J., Métris, G., Selig, H., Traon, O. L., Bresson, A., Zahzam, N., et al. (2016). Gravitation and geodesy with inertial sensors, from ground to space. *Aerospace Lab*, *12*, 1–16. https://doi.org/10.12762/2016.AL12-11

Touboul, P. J., Willemenot, E., Foulon, B., & Josselin, V. (1999). Accelerometers for CHAMP, GRACE and GOCE space missions: Synergy and evolution. *Bollettino di Geofisica Teorica ed Applicata*, *40*, 321–327.

Zingerle, P., Romeshkani, M., Haas, J., Gruber, T., Güntner, A., Müller, J., & Pail, R. (2024). Supplementary data to publication "The benefits of future quantum accelerometers for satellite gravity missions". [Dataset]. *Technical University of Munich*. https://doi.org/10.14459/2024mp1737747